CHAPTER NINE

# Stretch and poke stimulation for characterizing mechanically activated ion channels

**Amanda H. Lewis and Jörg Grandl***
Department of Neurobiology, Duke University Medical Center, Durham, NC, United States
*Corresponding author: e-mail address: grandl@neuro.duke.edu

## Contents



## Abstract

Quantitative functional characterization of mechanically activated ion channels is most commonly achieved by a combination of patch-clamp electrophysiology and stimulation by stretch (or pressure-clamp) and poke (or cell-indentation). A variety of stretch and poke protocols can be used to make measurements of many ion channel properties, including channel number, unitary conductance, ion selectivity, stimulus threshold and sensitivity, stimulus adaptation, and gating kinetics (activation, deactivation, inactivation, recovery from inactivation). Here, we review the general methods of stretch and poke stimulation and discuss the advantages and disadvantages of each. We use the vertebrate mechanically activated ion channel Piezo1 to explain equipment components and calibration, demonstrate experimental protocols and data analyses, and discuss underlying concepts and mechanistic interpretations.

*Methods in Enzymology*, Volume 654
ISSN 0076-6879
https://doi.org/10.1016/bs.mie.2020.12.024

## 1. Introduction

Characterizing the function of mechanically activated ion channels (MACs) is important for understanding the underlying mechanisms of their gating and ion permeation. However, analyzing the activity of MACs is less straightforward than that of channels activated by other stimuli, such as voltage or ligands: While the channel response (current) can be detected with high precision via patch-clamp electrophysiology, the physical stimuli (force, membrane tension) are comparatively difficult to measure, much less control. Sophisticated methods for mechanical stimulation have been developed, including magnetic force actuators, optical tweezers, ultrasound, fluid flow, and micropillar deflection, but use of these methods is not universal (Poole, Herget, Lapatsina, Ngo, & Lewin, 2014; Prieto, Firouzi, Khuri-Yakub, & Maduke, 2018; Ranade et al., 2014; Wu, Goyal, & Grandl, 2016; Ye et al., 2018). Rather, nearly all laboratories studying MACs use the two stimulation methods of stretch (or pressure-clamp) and poke (or cell-indentation). Widespread use of poke and stretch has arisen because both methods were invented early, are relatively easy to implement using commercially available equipment, and above all, because all validated MACs respond robustly to one or both assays (Awayda, Ismailov, Berdiev, & Benos, 1995; Coste et al., 2015; Coste, Crest, & Delmas, 2007; Deng et al., 2020; Hao & Delmas, 2011; Jia et al., 2020; Murthy et al., 2018; Patel et al., 1998; Sukharev, Martinac, Arshavsky, & Kung, 1993). As such, responsiveness to stretch and/or poke has become a standard for testing novel MAC candidates.

While the methods of stretch and poke are not difficult to learn, they each have limitations and pitfalls that may not be obvious and that can impact the analysis and interpretation of the data they generate (Table 1). The intention of this guide is to assist researchers in learning and mastering these methods with the specific goals of increasing experimental rigor and data quality. Specifically, we discuss the capabilities and inherent limitations of combining stretch and poke stimulation with patch clamp electrophysiology. We introduce the most important equipment components and how to properly calibrate and use them. We outline methods for designing protocols for standard characterizations of MACs function, accompanied by example data recorded in our lab from Piezo1, a voltage-dependent and inactivating MAC. Finally, we discuss choices of biological controls, technical quality checks, and how to properly triage, analyze, and interpret data. In summary, we hope this guide enables better comparison of results across laboratories, and thus ultimately improves mechanistic insight into MACs.

**Table 1** Comparison of stimulation paradigms.

| | Stretch stimulation | | Poke stimulation |
|---|---|---|---|
| **Patch configuration** | **Cell-attached** | **Inside-out, outside-out** | **Whole-cell** |
| Learning | Easy (few hours) | Moderate (few days) | Hard (few weeks) |
| Throughput | Very high (~dozens/day) | Lower (15/day) | Lower (15/day) |
| Solution control | Extracellular only | Intracellular and extracellular | Intracellular and extracellular |
| Membrane creep | Yes: potentially skewing the stimulus | No: finite membrane | n/a |
| Membrane potential | Intrinsic membrane potential is unknown | Exactly known and controlled by the amplifier | Exactly known and controlled by the amplifier |
| Preparation | Small to large-sized cells, blebs, vesicles, liposomes | Small to large-sized cells, blebs, vesicles, liposomes | Medium to large-sized cells |
| Stimulus quantification | Pressure is known; membrane tension can be determined indirectly by imaging | Pressure is known; membrane tension can be determined indirectly by imaging | Precise indentation depth; force and membrane tension are unknown |

## 2. Stretch or pressure-clamp stimulation

### 2.1 The stimulation paradigm

The principle of stretch stimulation is to apply air pressure to the inside of a glass pipette that holds a patch of membrane containing MACs. Increasing pressure both induces global membrane curvature as well as increases lateral membrane tension in the patch dome, either of which could, in principle, activate MACs (Fig. 1A). The method can be applied to large and medium-sized cells, cell blebs, vesicles, oocytes, and even reconstituted channels in artificial liposomes and lipid bilayers. The patch configuration can be cell-attached, inside-out or outside-out, and the air pressure can be positive or negative, providing great flexibility to probe MACs in multiple ways. Because patches are of relatively small membrane area (on the order of 1–2 $\mu m^2$), they contain few channels and are generally low noise, which allows for the resolution of single-channel gating events and access to the unitary conductance ($g$). The pressure clamp also provides

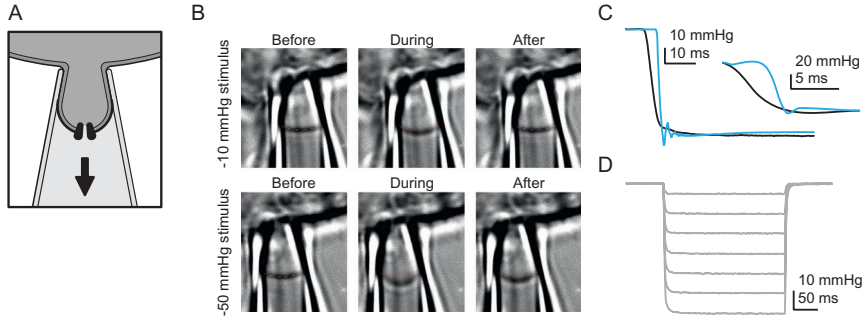


**Fig. 1** Stretch (or pressure-clamp) stimulation. (A) Schematic showing a cell-attached patch recording with negative pressure (suction) applied through the patch pipette. (B) Images of a cell-attached patch from a HEK293t cell. 300 ms pressure pulses were applied; images were captured immediately before, during, and after the pressure step. Holding potential was −80 mV. The red line indicates the location of the patch dome prior to the pressure step. Note that under low pressures (−10 mmHg), little creep occurs at negative potentials, but at higher pressures (−50 mmHg) the pressure step can be irreversible, such that the patch dome creeps further up the pipette. (C) Comparison of pressure steps from two differently tuned pressure clamp systems. The pressure step in black has a slower rise, but a smoother overall shape, whereas the pressure step in blue peaks sooner, at the expense of small oscillations (~10% of the maximum value). (D) Example of a full pressure step protocol from a well-tuned pressure clamp.

a reasonably quantitative means of comparing stimulus sensitivity across cells, channels, and/or conditions. Although the actual physical stimulus of membrane tension is not known in the stretch stimulation paradigm, it can be estimated indirectly by imaging the deformation of the membrane dome inside the patch pipette and using Laplace's law to calculate tension (Sokabe, Sachs, & Jing, 1991). We know from such imaging experiments that there is a non-zero membrane tension in the absence of pressure stimulation, and that repeated or extended duration of pressure can lead to a drift in both baseline and pressure-evoked membrane tension (Lewis & Grandl, 2015).

## 2.2 Patch configurations

The cell-attached configuration is easy to learn and quick to perform, such that trained electrophysiologists are able to perform dozens of individual experiments in a single day. Importantly, in this configuration the cytoskeleton and intracellular components, which may be integral to channel function, are largely unperturbed. Potential pitfalls of the cell-attached configuration are that the condition of constant membrane area can be violated by an effect called membrane creep (Fig. 1B), which is the lateral

movement (rather than bending due to pressure) of the patch dome further inside the patch pipette owing to the membrane adhesion energy and the ample supply of lipids from the cell. Creep can result in a change in the membrane area, and thus the absolute number of MACs exposed to the stimulus, as well as the relationships between pressure, membrane curvature, and membrane tension. Membrane voltage and the pressure stimulus itself have been identified as the major drivers of membrane creep and therefore need to be considered carefully when designing experimental protocols (Slavchov, Nomura, Martinac, Sokabe, & Sachs, 2014; Suchyna, Markin, & Sachs, 2009). In the following we discuss how to design protocols that minimize creep and thus enable the precise measurement of pressure-response curves and channel gating kinetics. In addition, neither the intracellular solution nor the intrinsic membrane potential can be controlled in the cell-attached configuration, which limits measurements of ion selectivity.

In contrast to cell-attached patches, the principal advantage of excised patch configurations (inside-out and outside-out) is that solutions on both sides of the membrane can be controlled, which allows for measuring the relative permeability of different ions. Additionally, the membrane patch area and correspondingly the number (N) of MACs remain constant throughout each experiment, as there is not a constant supply of new membrane. As a consequence, the measured current ($I$) remains directly proportional to the open probability $P_o$ even over the duration of long experiments, which allows for accurate normalization of stimulus-response curves and subsequent comparison across individual experiments. Downsides of excised patches include the potential effects of depletion of membrane or cytoskeletal components, such as PIP2, that may play a key role in channel function (Gamper & Rohacs, 2012). Additionally, excised configurations require greater experimental skill, which results in a longer training period and overall lower throughput. Below, we focus on protocols designed for cell-attached recordings from HEK293t cells and negative pressure, as this is the most common preparation, but in principle, they can be easily adapted for excised patches and other preparations as well.

## 2.3 Instrument setup and calibration

The High-Speed Pressure Clamp from ALA Scientific is the most widely used commercial system for stretch stimulation (Besch, Suchyna, & Sachs, 2002). It provides sufficient stimulus amplitude (±200 mmHg) and resolution (±0.3 mmHg) for all MACs, biological systems, and protocols that we

are aware of. However, its control speed of 5–15 ms is slow compared to the kinetics of some channel gating transitions, especially that of activation, which for many channels is sub-millisecond. The control speed also depends on the stimulus amplitude, which needs to be considered for certain experimental protocols. The responsiveness of the pressure-clamp system can be tuned by the manufacturer to optimize speed, overshoot, and oscillations, which are competing effects. We recommend periodically checking the performance and having the instrument recalibrated when deviations are detected. The pressure clamp is powered by a vacuum pump, which should also be monitored routinely for optimal performance. Equally important, to optimize performance, the pressure clamp must be connected to the microelectrode holder with thick-walled silicone tubing that is not longer than 10 cm. A well-tuned pressure-clamp system should deliver pressure profiles similar to that shown in Fig. 1C and D.

The exact geometry of the patch pipette also shapes how the membrane dome curves under applied pressure. Therefore, great care must be taken to produce patch pipettes of consistent shape. In particular, for tension-gated channels, owing to Laplace's law ($T = R^*\Delta P/2$; where T = tension, R = radius, P = pressure), patch pipettes with a larger size and thus a larger patch dome radius will have a left-shifted $P_{50}$ curve. Therefore, monitoring the pipette resistance and using this value to triage experiments can be an effective strategy to produce results of higher consistency.

### 2.3.1 Controls

*Negative controls*: As all cells are inherently mechanosensitive to some degree, background (endogenous) expression of mechanosensitive ion channels is a serious concern, particularly when characterizing putative novel MACs (Dubin et al., 2017). Therefore, appropriate negative controls must be performed to ensure activity truly arises from the channel of interest. These should include, (1) recordings from cells that are mock transfected (when recording heterologously expressed channels) or treated with siRNA against the channel of interest (when recording natively expressed channels), and (2) the addition of specific inhibitors or channel blockers (such as ruthenium red or gadolinium for Piezo1) to the patch pipette. For single-channel measurements, including unitary conductance, it is also critical to confirm that channel activity is time-locked to the stimulus to reduce potential contamination from other background, non-mechanosensitive ion channels.

*Positive controls*: Positive controls will depend on the precise experiment but are useful to ensure proper setup of the pressure clamp system. These

could include recording from channels with a known $P_{50}$ or with well-characterized gating kinetics to confirm correct calibration and speed of the pressure clamp, respectively. For polymodal channels, an additional positive control for determining channel number (N) is activating channels with a non-mechanical stimulus, such as voltage or chemical ligand, known to achieve $P_o \sim 1$.

## 2.4 Experimental protocols

### 2.4.1 *Unitary conductance* g

Knowing the unitary conductance of a particular channel gives key insight into the properties of the channel pore. We recommend calculating slope, rather than chord conductance, for two reasons: (1) In a cell-attached patch, the membrane potential is not known, even in a high-potassium bath intended to shift $E_m$ to 0 mV, and (2) this does not require prior knowledge of the reversal potential in the chosen buffers. To measure slope conductance, one must measure the unitary current ($i$) of single channel activity at several applied potentials. Since the total number of channels differs in each individual patch, the pressure stimulus needs to be titrated such that at most times only zero or one channel is open. Downstream data analysis is most accurate if recordings contain ~50% baseline (no channels open) and ~50% activity (one channel open). This goal is best achieved by regulating the pressure stimulus on the fly, either by using the manual dial on the High-Speed Pressure Clamp or via software, while recording current continuously at a constant holding potential. In order to maximize patch stability and thus recording time, we recommend working from lower pressure stimuli towards higher values. For Piezo1, less than −10 mmHg is typically required to elicit the desired level of activity and in a subset of patches, particularly those with large numbers of low-threshold channels, resting tension is sufficient to elicit a small level of activity.

An accurate and unbiased analysis entails the following steps (Fig. 2):

**(1)** Generate current amplitude histograms from selected recorded segments that are stable (no baseline drift) and contain ~50% baseline and ~50% channel activity (Fig. 2A).

**(2)** Fit the current amplitude histograms with double Gaussian curves. The difference in the midpoints of both Gaussians is the current amplitude $i$ and the width of the broader of the two Gaussian distributions should be taken as standard deviation $\sigma(i)$. The histogram may also indicate whether increasing the low-pass filtering of current recordings is necessary in order to better resolve channel openings (Fig. 2B).

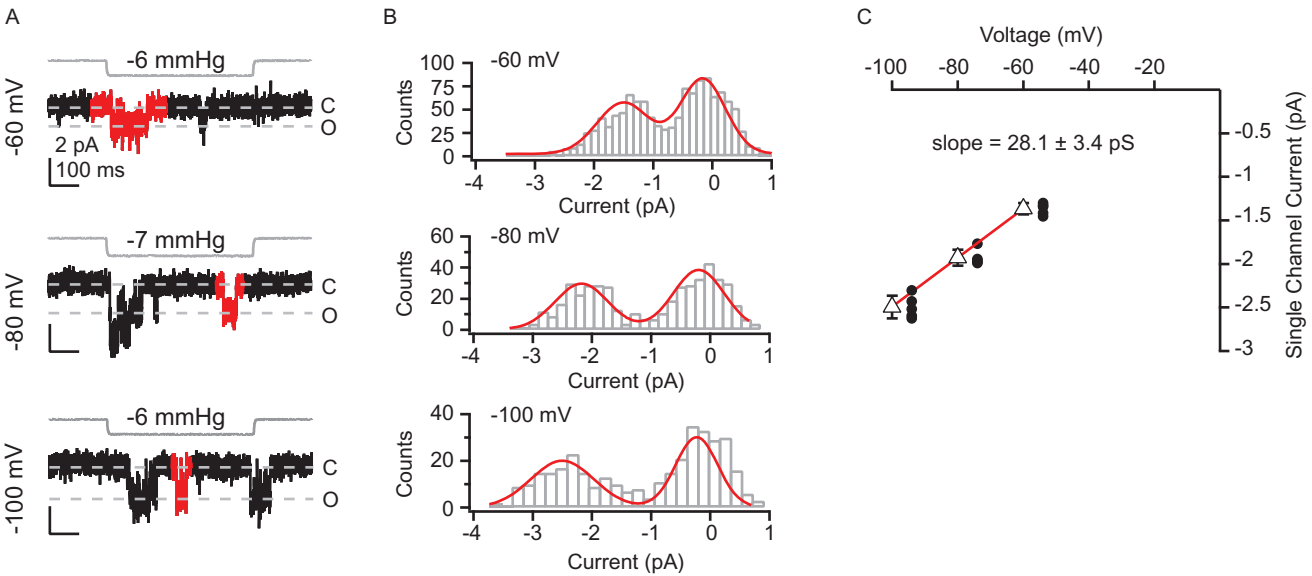


**Fig. 2** See figure legend on opposite page.

**(3)** Fit the current amplitude levels $i$ as a function of the holding potential V for each individual cell with a line, while taking the standard deviation $\sigma(i)$ into account. The slope of the line fit is the unitary conductance $g$ and the slope error is its standard deviation $\sigma(g)$. For recordings in the cell-attached configuration, it is absolutely crucial to determine the conductance $g$ for each individual cell before averaging $g$ values across experiments, because even in a high-potassium bath, the intrinsic membrane potential can differ for each cell and alter absolute current levels. Also note that slope conductance can vary with voltage in channels that rectify, so care should be taken to ensure the fit remains linear throughout all voltages (Fig. 2C).

**(4)** Average all $g$ values of individual cells, while taking the standard deviation $\sigma(g)$ into account.

*Replication*: For a rigorous analysis, this procedure should be repeated for 5–7 openings at each of 3–6 holding potentials per patch. The mean conductance should be calculated from 5 to 10 individual patches, spanning at least 2 individual transfections or preparations.

**Fig. 2** Unitary Conductance. (A) Pressure protocol (gray) and current (black) from a cell-attached patch of a HEK293t cell expressing human Piezo1. Sweeps were obtained at three voltages: −60 mV (top), −80 mV (middle) and −100 mV (bottom). Openings used to generate all-points histograms are highlighted for each sweep in red; the baseline on either side of the opening was chosen such that peaks have equivalent areas. (B) All-points histograms generated from current sweeps in (A). Binning was calculated using the Freedman-Diaconis method and an optimal bin width of $2*\mathrm{IQR}(x)/N^{1/3}$, where IQR is the interquartile distance, N is the number of observations, and the bins are evenly distributed between the minimum and maximum values. Red lines indicate a double-Gaussian fit to binned data using the equation:

$$y = y_0 + A_1 * e^{-\left(\frac{x-x_1}{w_1}\right)^2} + A_2 * e^{-\left(\frac{x-x_2}{w_2}\right)^2}$$

where $y_0$ is the baseline current, $A_1$ and $A_2$ are the peak amplitudes, $w_1$ and $w_2$ are widths, and $x_1$ and $x_2$ are the centers of the fits. The difference between $x_1$ and $x_2$ reflects the difference between mean current in the open and closed state and is used to calculate single channel current. (C) Single-channel current amplitude plotted as a function of voltage. Each black circle is the single-channel current amplitude for one opening at that voltage ($n = 5$–7 openings per voltage), triangles represent mean ± standard error. The slope of a linear fit, weighted by the standard errors, yields the single-channel conductance ± standard error.

### 2.4.2 Channel number N

Determining the number of ion channels (N) in an individual patch is one means of estimating channel expression levels. It can also be used as a quality control step in other experiments (see below). N can be calculated by stimulating the patch with a saturating pressure step to simultaneously open all channels and achieve maximal current amplitude $I_{max}$, which is then divided by the single channel conductance to obtain

$$N = \frac{I_{max}}{g * V}$$

Importantly, reliable calculation of N relies on the assumption that open-probability $P_o = 1$ can be achieved, which may not be valid for all MACs, particularly those which inactivate rapidly. It is therefore important to understand all factors that may influence the open probability of a probed MAC, such as voltage-dependence, pressure sensitivity, and gating kinetics, and design the protocol accordingly such that the test stimulus maximizes $P_o$ while minimizing creep (Fig. 3).

*Replication*: Since channel density is highly heterogeneous and patch surface areas can vary even for identical pipettes by a factor of ~2, the channel number N will vary dramatically from patch to patch. Therefore, in order to use this measurement as a proxy for surface expression levels it must be repeated very often ($N > 50$) and with care to control pipette shape and size to maximize consistency across experiments. For individual patches, N can be calculated before and/or after the protocol of interest; in fact, comparing N pre- and post- stimulus may serve as an important control and give insight into the level of patch creep resulting from a given protocol. For polymodal channels that can also be fully activated by a non-mechanical stimulus, such as voltage or a chemical ligand, this stimulus can be used as a positive control.

### 2.4.3 Pressure-response curves ($P_{50}$)

One of the most common characterizations for MACs is the stimulus-response or $P_{50}$ curve, which is an indirect measurement of the response range of the channel to force. In principle, the response at each stimulus intensity can be normalized to the total number of channels in the patch (N), and subsequently measurements from different cells can be averaged to ultimately yield stimulus-response relationships that are very precise. However, for this normalization and subsequent averaging to be valid, three conditions must be fulfilled: (1) The stimulus protocol must be designed

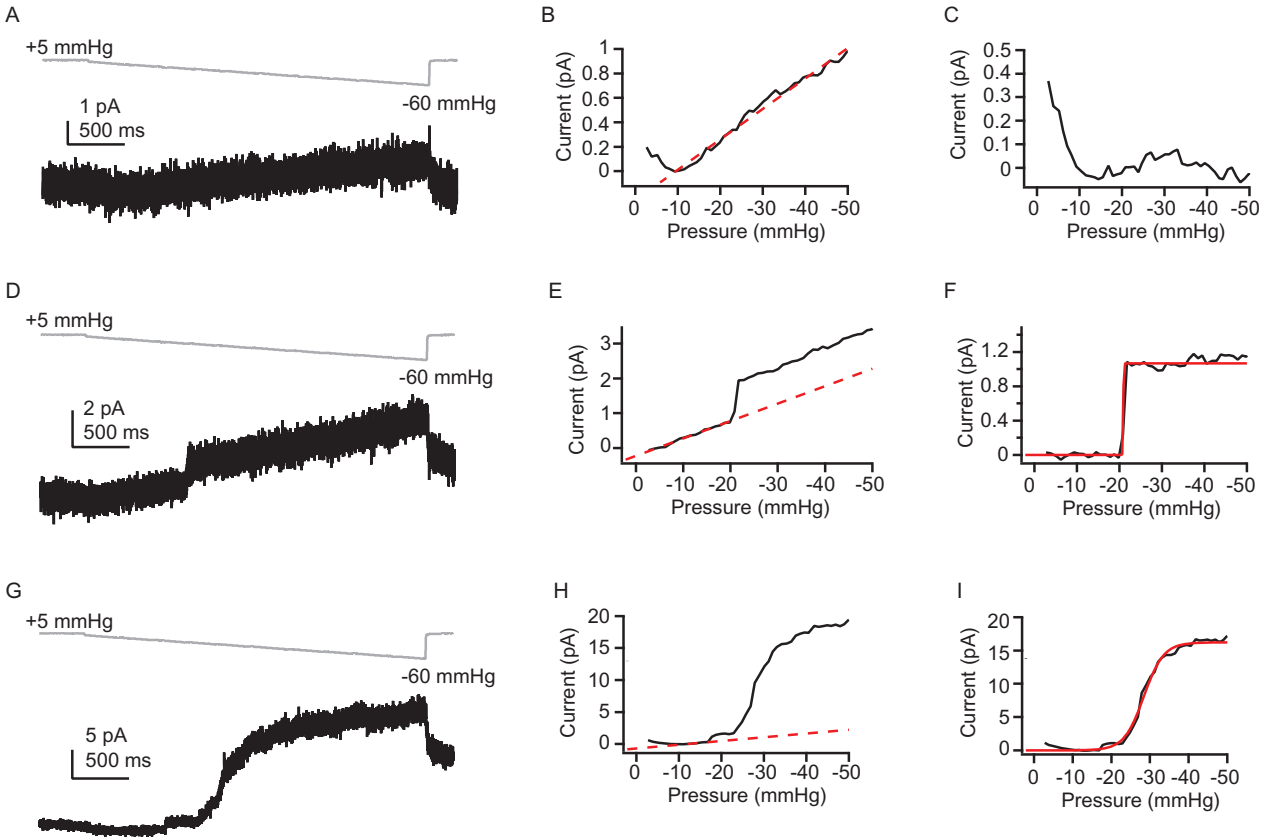


**Fig. 3** See figure legend on next page.

such that each single stimulation is not affected by previous stimuli. This means that each stimulus must be short to minimize membrane creep and ensure reversibility, and that the inter-stimulus interval must be long enough to allow for recovery from potential inactivation. Additionally, the patch should be held at negative potentials between sweeps to minimize voltage-dependent creep. Practically, reversibility can (and should) be verified by demonstrating that exposure to repeated stimuli of identical amplitude yields identical responses. (2) Each individual response curve must clearly reach saturation. Non-saturating patches will skew the averaging and must therefore be triaged. The mean stimulus response curve must also show saturation, which is a straightforward quality check for experimenters and peer reviewers. (3) In order to ensure measurements are good

**Fig. 3** Channel number (N). (A) Pressure protocol (gray) and current (black) from a cell-attached patch from a HEK293t cell expressing mouse Piezo1. Holding potential was +60 mV to minimize inactivation. Pressure was increased stepwise from +5 mmHg to −60 mmHg in 1 mmHg steps, 50 ms per step. Pressure was clamped at +5 mmHg for 1 s prior to the step protocol to remove resting tension from the patch. (B) Current-pressure relationship for the patch in (A). Mean current was calculated for each step, in 1 mmHg increments, and plotted as a function of pressure. Note the linear relationship between current and pressure during the step, despite no channel activity in this patch (inferred from the lack of discrete channel opening event). This is likely due to small changes in seal quality and/or capacitance. The linear portion of the current-pressure relationship was fitted with a line (red dashes). (C) As in (B) after subtraction of the current corresponding to the fitted line. (D) As in (A) for a patch with 1 channel. (E) Current-pressure relationship for the patch in (D). The linear portion of the current-pressure relationship prior to the first opening was fitted with a line (red dashes). (F) Current-pressure relationship for the patch in (D), with the change in current due to leak changes (red dashed line in E) subtracted. The resulting current was fitted with the following equation:

$$I = I_{min} + \frac{I_{max}}{1 + e^{\left(\frac{P50-P}{k}\right)}}$$

where $I$, $I_{min}$, and $I_{max}$ are current, minimum current, and maximum current, $P$ is pressure, $P_{50}$ is half-maximal pressure and $k$ is slope. From the fit (red line), $I_{max}$, which corresponds to single-channel current, was 1.1 pA and $P_{50}$ was 20.9 mmHg. (G) As in (A) for a patch with many channels. (H) Current-pressure relationship for the patch in (G). The linear portion of the current-pressure relationship prior to the first opening was fitted with a line (red dashes). (I) Current-pressure relationship for the patch in (D), with the change in current due to leak (red dashed line in H) subtracted. From a sigmoidal fit to the data (red line) P50 was calculated to be 28.4 mmHg, slope was 2.56 mmHg, and $I_{max}$ was 16.2 pA. Approximate number of channels in this patch can further be calculated by dividing $I_{max}$ by mean single channel current (~1 pA), and is 16 channels.

representations of channel ensembles and not skewed by the quantified nature of unitary conductance and the stochasticity of channel gating, each individual patch should reach a predefined $I_{max}$ value (we recommend $N > 25$ channels).

The most pertinent outcome of a pressure-response curve is the pressure of half-maximal activation ($P_{50}$), which is a proxy for the mechanical sensitivity of the MAC. Since a sigmoid fit to the data uses four free parameters ($I_{baseline,}$ $I_{max}$, $P_{50}$, and slope) high quality curves should be based on >8 distinct pressure amplitudes, with an equal number of points below and above the $P_{50}$ value. Importantly, while it is tempting to first average individual pressure-response curves and then fit mean data, the slope will be skewed (towards larger values, i.e., less steep) by the averaging of individual curves with varying $P_{50}$ values. Therefore, first fitting slopes of all individual pressure-response curves, and subsequent averaging is a better way to assess the true steepness.

Our lab has shown that for inactivating MACs, pressure-response curves are systematically shifted by resting membrane tension, which is present in any membrane patch even in the absence of a pressure stimulus. This deviation can be compensated for by applying a non-zero baseline pressure that minimizes resting tension for a sufficient amount of time to allow channels to recover from inactivation (Lewis & Grandl, 2015).

Generating a stimulus-response curve entails the following steps (Fig. 4):

1. Triage all individual experiments that do not clearly exhibit saturation or a predefined $I_{max}$ value. We recommend that current responses to the highest three stimulus amplitudes should deviate by less than 10% and that $I_{max}$ corresponds to $N > 25$ channels, respectively (Fig. 4A, B)
2. Normalize each individual response curve to the maximal response, $I_{max}$ (Fig. 4C).
3. Fit individual curves with a sigmoid function to obtain $P_{50}$ and slope values.
4. Calculate mean $P_{50}$ and slope values and, if desired, generate a simulated curve based on mean parameters.

*Replication*: Stimulus-response curves should be based on at least 10 individual patches and 2 individual transfections/preparations.

### 2.4.4 Adaptation

Current decay during prolonged stimulus application may be the result of channel-intrinsic inactivation (the MAC adopts a non-conducting state), stimulus adaptation (the local force on the channel dissipates over time),

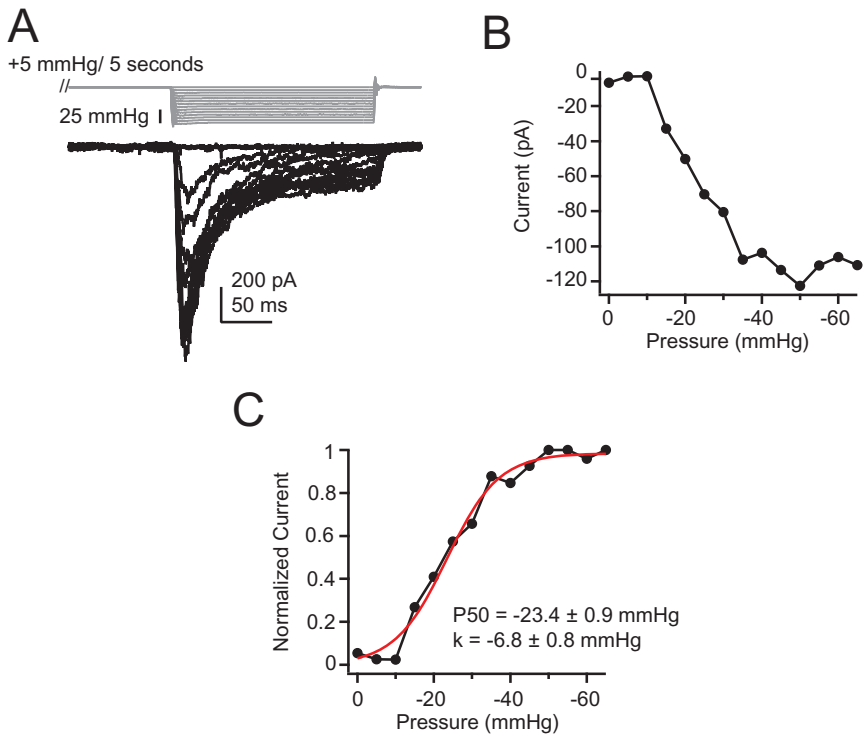


**Fig. 4** Pressure-response curves. (A) Pressure protocol (gray) and current (black) from a cell-attached patch from a HEK293t cell expressing mouse Piezo1. Holding potential was −80 mV. Pressure was clamped at +5 mmHg for 5 s prior to the pressure-step to minimize resting tension and thus inactivation. (B) Peak current amplitude as a function of voltage for the cell in (A). (C) Pressure-response curve for the cell in (A) normalized to the maximum response for that patch. Current-pressure relationship was fit with the following equation (red):

$$I = I_{min} + \frac{I_{max}}{1 + e^{\left(\frac{P50-P}{k}\right)}}$$

where $I_{min}$ and $I_{max}$ are normalized minimum and maximum current values, $P$ is pressure, $P_{50}$ is half-maximal pressure, and k is the slope.

or both. The respective contributions can be estimated in the following way (Fig. 5):

1. Apply a test pulse to a saturating pressure to assess maximum current for the patch ($I_{\text{max,unconditioned}}$) (Fig. 5A).
2. Apply a conditioning pressure step that is both saturating and long compared to the kinetics of overall current decay, ideally resulting in

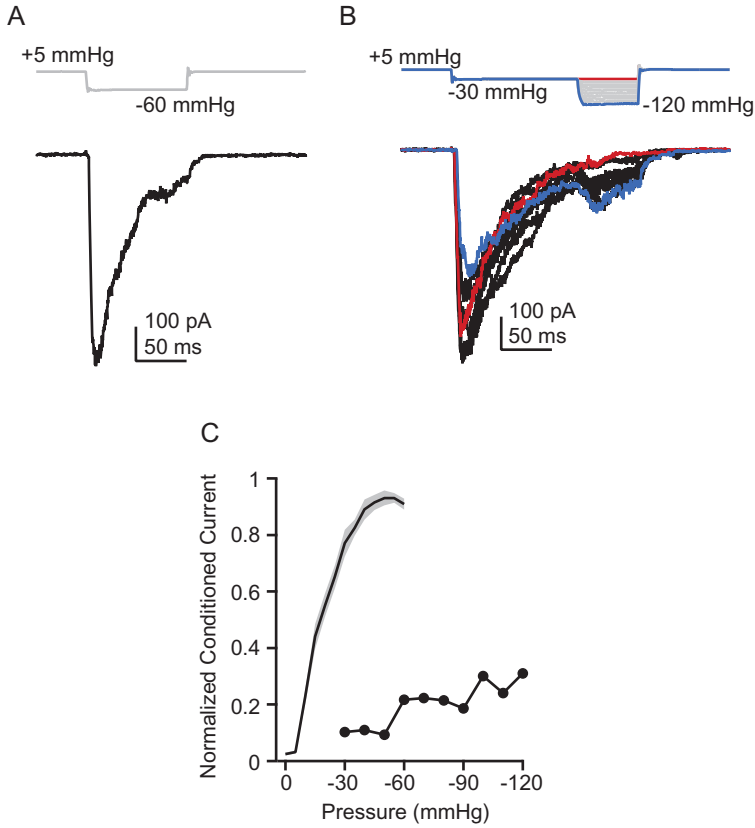


**Fig. 5** Adaptation. (A) Single, saturating pressure step to −60 mmHg (gray) and corresponding current (black) from a cell-attached patch from a HEK293t cell expressing mouse Piezo1. (B) Adaptation pressure protocol (gray) and currents (black) from the same cell as in (A). The protocol was designed to have a single, near-saturating conditioning pulse to −30 mmHg, followed by a test pulse to higher pressures. (C) Black circles are peak current amplitudes upon the conditioning pulse from (B) normalized to the maximal peak current amplitude during the initial saturating pulse (A), as a function of pressure. The black line is the current-pressure response from many cells ($n = 11$), with the standard error shaded in gray. The low amplitude of peak currents upon increased pressure after conditioning indicate that the current is predominantly inactivating, rather than adapting.

a stable plateau current representing equilibration among gating states. The conditioning step is directly followed by a second brief (test) pressure step of larger and varying magnitude (Fig. 5B).

2. Fit the peak current amplitudes evoked by the test step as a function of pressure amplitude with a sigmoid function (Fig. 5C). The current

amplitude and $P_{50}$ evoked by the second (test) stimuli ($I_{max,test}$, $P_{50,test}$) can be compared to those of an unconditioned pressure-response curve ($I_{max,unconditioned}$, $P_{50,unconditioned}$). If $I_{max,test} \ll I_{max,unconditioned}$, then current decay is driven predominantly by channel-intrinsic inactivation rather than adaptation. If however, $I_{max,test} \sim I_{max,unconditioned}$, AND if $P_{50,test} \gg P_{50,unconditioned}$, then current decay is driven to some extent by stimulus adaptation.

*Replication*: Measurements should be based on at least 10 individual patches and 2 individual transfections/preparations.

### 2.4.5 Gating kinetics: Activation, deactivation, inactivation, recovery from inactivation

Measuring the kinetics of channel gating can provide deep insight into the mechanisms of activation (opening upon stimulation), deactivation (closing upon stimulus removal), and inactivation (pore occlusion during prolonged stimulus exposure). The principal difficulties common to determining each of these gating transitions are that the initial state of the channel population is typically not homogenous (e.g., not all channels are in the resting state before stimulating), and that the gating transitions may be hard to separate (i.e., current decay (pore occlusion) can originate from deactivation or inactivation). Also, as for measurements of pressure sensitivity, only patches above a predefined $I_{max}$ value provide good average representations of channel gating and should be used for analysis (we recommend that $I_{max}$ corresponds to $N > 25$ channels). Finally, developing a suitable protocol for one gating transition may require knowing time constants of the other transitions and systematic tuning of protocols to pre-populate channels in the desired state. For a prototypical inactivating MAC, this entails the following (Fig. 6):

**Activation**

1. Apply an activating pressure step of saturating amplitude. For inactivating channels, this step should be preceded by a non-zero baseline pressure that minimizes resting tension for $\sim 3\times$ the time-constant of recovery from inactivation, in order to populate a maximum of channels in the resting state (Fig. 6A).
2. Fit the current peak with an exponential function to determine the activation time constant ($\tau_a$). If the current inactivates AND if the time constant of inactivation is similar to that of activation, the current should instead be fit with a double exponential to capture both time constants.

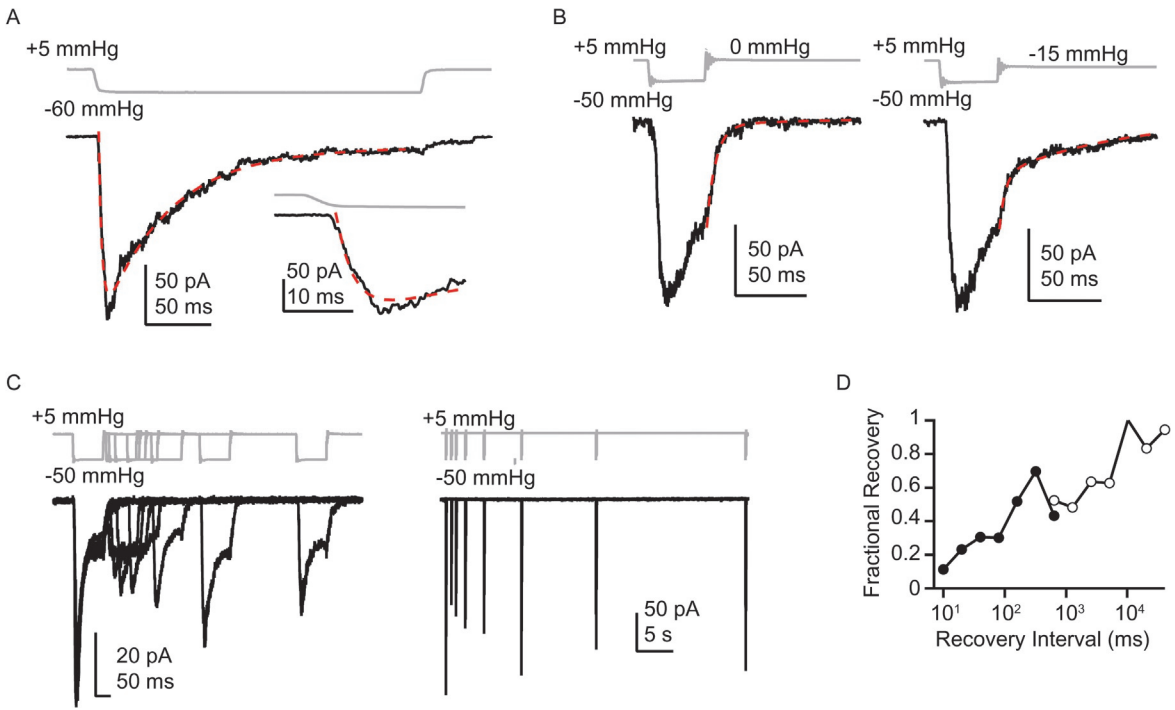


**Fig. 6** See figure legend on next page.

3. Only activation time constants that are much slower (~3×) than the pressure stimulus rise time, which is ~15 ms, accurately reflect channel gating; otherwise, the time constant measured is a lower bounds on the speed of gating.

**Deactivation**

1. Apply a saturating pressure step that is short (~1/3×) compared to the time constant of inactivation to maximize the number of open channels, followed by a step to lower pressures that favors channel closure (Fig. 6B).

**Fig. 6** Gating kinetics. (A) Pressure protocol (gray) and current (black) from a cell-attached patch from a HEK293t cell expressing mouse Piezo1. Holding potential was −80 mV. Pressure was clamped at +5 mmHg for 5 s prior to the pressure step to minimize resting tension and thus inactivation. Current was fit with a double exponential of the form:

$$y = y_0 + A_1 * e^{\frac{-(x-x_0)}{\tau_1}} + A_2 * e^{\frac{-(x-x_0)}{\tau_2}}$$

where $y_0$ is steady-state current, $\tau_1$ and $\tau_2$ are exponential time constants of activation and inactivation and $A_1$ and $A_2$ are their corresponding amplitudes. For the current in (A) the $\tau$ of activation was 2.5 ms and of inactivation was 50.6 ms. Inset shows activation portion of the current response at a magnified time scale; note that activation is fast relative to the onset of the pressure step, and therefore the activation $\tau$ should be interpreted with caution. (B) Pressure (gray) and corresponding currents (black) from a HEK293t cell expressing mouse Piezo1. The protocol designed to measure deactivation via an initial brief, saturating pulse to −50 mmHg to open channels but not allow for substantial inactivation, followed by steps to 0 mmHg (left) or −15 mmHg (right) to measure rates of transition to closed (left) or mixed closed/inactivated (right) states. The current on the left was well-fit with a single exponential equation; $\tau = 6.3$ ms. The current on the right was well-fit with a double exponential equation; $\tau_1 = 4.0$ ms and $A_1 = 50\%$; $\tau_2 = 71.1$ ms and $A_2 = 50\%$. In this case, because the return pressure step is near the $P_{50}$ for this channel, current decay reflects channels both deactivating ($\tau_1$) and inactivating ($\tau_2$). (C) Pressure step (gray) and currents (black) from two separate HEK293t cells expressing mouse Piezo1. The two step recovery protocol features an initial pressure step to −50 mmHg to open and inactivate channels, followed by varying intervals of recovery at +5 mmHg (~10 ms to 20 s) and a subsequent second pulse to −50 mmHg to test the fraction of channels that recovered. The left protocol is designed to measure the fast component of recovery from inactivation and the right protocol is designed to measure the slow component of recovery from inactivation. (D) Fractional recovery, measured by the peak current during pressure step two as a fraction of peak current during pressure step one. Closed circles represent data from fast recovery protocol; open circles represent data from slow recovery protocol.

2. Fit the current decay following the pressure step with two exponential functions to determine the time constants of deactivation ($\tau_d$) and inactivation ($\tau_i$). The time constant identical to that determined with the inactivation protocol can be attributed to inactivation and the remaining time constant to deactivation. The relative contribution of the two time constants will depend on the pressure and corresponding fraction of channels that inactivate versus close. At very low pressures, nearly all channels will close, and current decay can instead be fit with a single exponential ($\tau_d$).
3. Only deactivation time constants that are much slower ($\sim 3\times$) than the stimulus decay time, which is $\sim 15$ ms, truly reflect channel gating.

**Inactivation**

1. Apply a saturating pressure step that is long compared to the kinetics of overall current decay (at least $3\times \tau_i$), ideally resulting in a stable current equilibrium (Fig. 6A).
2. Fit the current peak with two exponential functions (for current rise and decay) to determine the inactivation time constant ($\tau_i$). If inactivation is sufficiently slow compared to activation, the current can instead be fit with a single exponential.
3. Alternatively, inactivation can be characterized by quantifying the relative current decay post current peak amplitude (e.g., 30% decay after 200 ms). This method is especially suited for MACs that inactivate over timescales comparable to the stimulus duration, or lack inactivation entirely.

**Recovery from inactivation**

1. Apply two saturating stimuli at decreasing time intervals. This approach provides an opportunity for detecting run-up or run-down of channel activity unrelated to inactivation and can be used to triage experiments (Fig. 6C). It is important that the stimulus intervals span a wide range of durations and comprise values that are both much shorter and much longer than the observed time constant(s) of recovery.
2. Fit the peak current amplitudes from the second stimulus, normalized to the first stimulus, as a function of recovery time intervals with a single exponential; if the relationship is clearly multi-phasic then multiple exponentials should be used (Fig. 6D).

*Replication*: Time constants of gating kinetics should be based on at least 10 individual patches and 2 individual transfections/preparations. If channel run-up or run-down is an issue, consider splitting the protocol into two to separately measure fast and slow components of recovery, if necessary.

## 3. Poke or cell-indentation stimulation

### 3.1 The stimulation paradigm

In poke stimulation, a fire-polished glass pipette indents a cell that is simultaneously patched in the whole-cell configuration, allowing electrical access to the activity of all channels in the membrane (Fig. 7A). The evoked current amplitudes are typically about one order of magnitude larger as those evoked

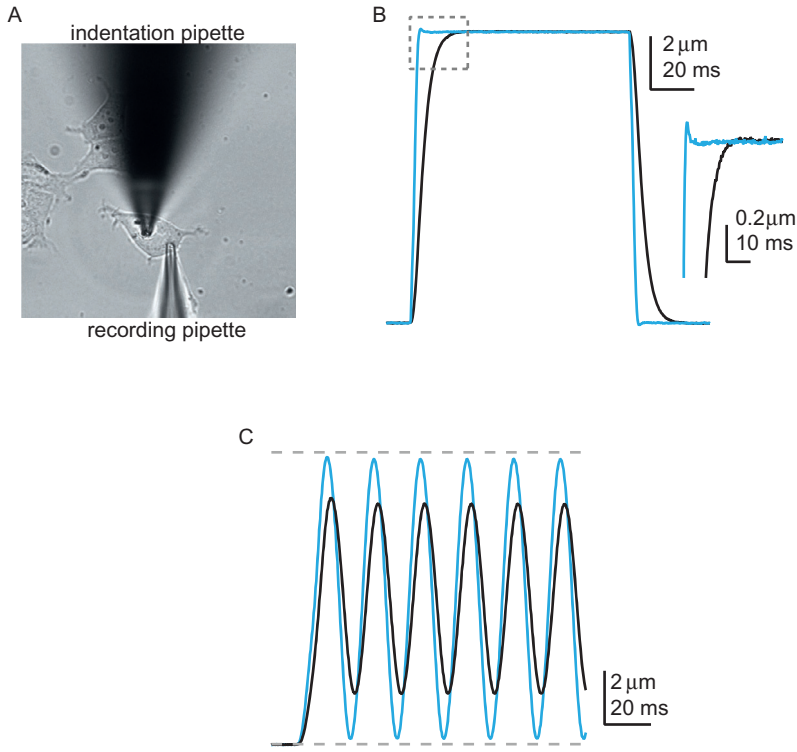


**Fig. 7** Poke (or cell indentation) stimulation. (A) Brightfield image of a HEK293t cell, an indentation pipette that has been fire-polished at the tip to a diameter of ~2 µm, and a recording pipette. (B) 10 µm indentation stimulus before (black) and after (blue) tuning to increase the speed of piezoelectric driver movement. Pipette movement was driven by an E-625 Piezo Servo Controller (Physik Instrumente) in closed-loop mode. To accelerate the rise, the slew knob was turned counter-clockwise and the gain loop was turned clockwise until the rise accelerated with minimal overshoot (<0.5 µm). The inset shows the boxed region. (C) 50 Hz stimulus from before (black) and after (blue) calibration. Note that with the slower settings, there is significant undershoot of the commanded 10 µm amplitude (gray dashes).

by stretch stimulation, because the activity of many more channels is recorded in the whole-cell configuration relative to a patch, and likewise the membrane area deformed by indentation is much larger. The large current amplitudes are advantageous for detecting MACs with low expression levels and/or low unitary conductance, or for measuring well-averaged gating kinetics of large channel ensembles. However, the concerted activity of many channels, as well as the increased noise of the whole-cell configuration, preclude analysis of single channel unitary conductance.

Poke stimulation is somewhat harder to learn and perform than stretch stimulation, because obtaining a whole-cell configuration and positioning the poke pipette in addition to the patch pipette requires more skill. Yields are correspondingly lower, in the range of 1–5 successful experiments per hour.

The principal difficulty in establishing stimulus-response relationships with poke is that the forces on the membrane induced by indentation and its resulting cell deformation are not only unknown, but also likely change non-monotonically with indentation depth, are unlikely to be equally distributed throughout the cell, and likely dissipate to some extent during the stimulus. Moreover, indentation-response curves rarely saturate before patch rupture, suggesting that increasing membrane area, and with it, channel numbers, are stimulated with each deeper poke, further complicating analysis of stimulus-response relationships. Even the point of first cell contact, and with it the exact indentation depth, cannot be determined with high precision, because it is usually only assessed visually. Taberner et al. pioneered a relatively simple method for measuring the point of first cell contact more precisely by monitoring the electric resistance of the stimulation pipette, but it has yet to be adopted widely among laboratories (Taberner et al., 2019). As a result, indentation-response relationships and current kinetics have to be analyzed and interpreted with caution, which we will discuss in detail.

## 3.2 Instrument setup and calibration

For fast and precise indentation, the poke pipette needs to be positioned and moved by a piezo-actuator, which is commercially available through several companies. Our lab uses the P-601.1SL from Physik Instrumente, driven by the E-625 Piezo Servo Controller and mounted to a micromanipulator (MPC-200; Sutter Instrument) with a custom-designed and fabricated bracket (JM Specialty Parts). This actuator achieves travel speeds of 0.5 μm/ms with 0.2 nm resolution, which is sufficient for achieving

indentation steps of 0.5–1 μm used by nearly all laboratories. Long travel range (~400 μm) is another important consideration when choosing an actuator, as it will greatly facilitate pipette positioning. The stimulation pipette should be fire-polished with a microforge (MF-830; Narishige) to a smoothly rounded ~2 μm tip (Fig. 7A).

Unstable mounting or poor piezo-actuator calibration can result in pipette vibrations that manifest as oscillations or "ringing" in the current signal, which can diminish data quality and downstream analysis. Calibration of the piezo-actuator depends on the exact weight and mass-distribution of the load, i.e., the poke pipette. We therefore recommend carefully calibrating the actuator and establishing methods for reproducible pipette mounting, such as pulling pipettes of consistent length and using markers for consistent pipette mounting. The piezoelectric controller can be manually tuned to achieve faster movement of the actuator, at the expense of oscillations and overshoots (Fig. 7B–C).

#### 3.2.1 Controls

*Negative controls*: As for pressure-clamp recordings, care must be taken to ensure activity is from the channel of interest by recording from cells that are mock-transfected, treated with siRNA against the channel of interest, and/or in the presence of channel blockers or inhibitors.

*Positive controls*: Positive controls include recording from MACs with known gating kinetics or permeation properties.

### 3.3 Experimental protocols

#### 3.3.1 Channel number (N) and indentation-response curves

While the number of MACs activated by a poke step can be simply calculated from the peak current amplitude $N = I_{max}/i$, the inability to evoke current saturation (or $P_o \sim 1$) before patch rupture prevents the accurate measurement of membrane expression levels or stimulus sensitivity. Consequently, if the MACs respond to stretch stimulation this paradigm should be preferred. However, poke stimulation can resolve stark differences in membrane expression, such as may be the consequence of genetic knockdown, or in sensitivity by reducing data averaging to a minimum (Fig. 8):

1. Use the piezo-actuator to advance the poke pipette in small increments (1 μm or less) to visually determine the minimal amplitude that evokes cell deformation; then use this amplitude value as a new baseline for further stimulation. This calibration will enable a rough comparison of stimulation-responses across different cells. The error should be

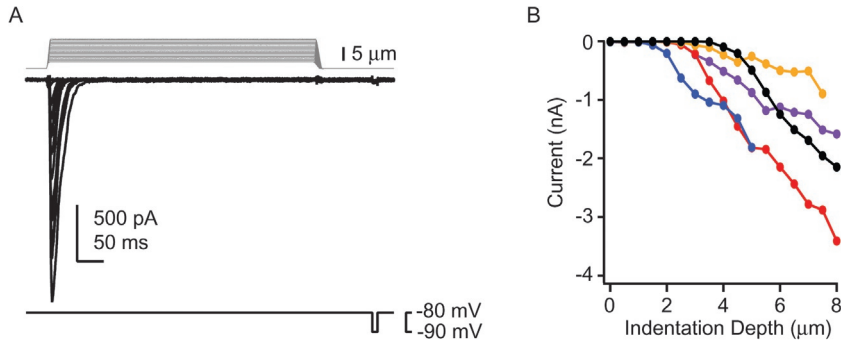


**Fig. 8** Channel number N and indentation-response curves. (A) Indentation stimulus protocol (top), current (black), and voltage protocol (bottom) from a whole-cell recording from a HEK293t cell expressing mouse Piezo1. The voltage protocol includes a brief hyperpolarizing step at the end of each sweep to check for changes in membrane seal and resistance. (B) Stimulus-response protocol for five separate cells. Absolute value of movement of the piezoelectric controller is corrected for the distance traveled at first touch, determined by eye, where 0 µm is first touch. The piezoelectric driver was advanced until the patch ruptured, evidenced by a nearly instantaneous increase in negative current that saturated the amplifier.

estimated to be at least ± the step increment, although experimenters should be aware that in reality it is likely 2× higher, because the visual cues for cell contact are subtle and can be easily missed.

2. Execute the indentation protocol with increasing step-size (e.g., 0.5 µm) until the patch ruptures. The time interval between indentations should be ~3× the time constant of recovery from inactivation (Fig. 8A).
3. Plot the entire indentation-response relationship separately for every individual cell, without averaging current amplitudes, perhaps using different colors or shades (Fig. 8B). The individual plotting accounts for the knowledge that each cell varies in size, shape, elasticity, and membrane expression level, all of which affect to what extent indentation evokes MAC activity. Plotting responses up to the very last executed stimulus reveals if cells are less tolerant to mechanical stimulation and experience seal rupture earlier. Of course, stimulus responses can also be displayed as averages across cells, knowing that responses due to variations in cellular properties are skewed and masked. Normalizing curves to their maximal response amplitudes should be avoided because individual patches rupture at different indentation depths.

*Replication*: Indentation-response curves should be based on at least 10 individual cells and 2 individual transfections. In addition, because the measurement involves the subjective estimate of first cell contact, the experimenter should be blinded to the experimental condition.

### 3.3.2 Ion-selectivity

The whole-cell configuration allows control of the membrane potential and both intracellular and extracellular solutions, and therefore permits measuring not only reversal potential, but also ion selectivity of MACs. However, precise determination of the reversal potential relies on highly reproducible stimulation amplitudes, which cannot be assumed a priori given that cells are partially inelastic. It is therefore important that cell indentation is performed and controlled carefully (Fig. 9):

1. Advance the piezo actuator in steps (~1 μm) in order to find an ideal stimulation amplitude. The goal is to indent the cell as little as possible in order to maximize patch stability while achieving current amplitudes that are large enough to provide good statistical averaging of stochastic channel gating.
2. Repeatedly poke the cell at the same predetermined indentation depth, while varying the holding potential. We recommend a minimum of 5 different potentials (e.g., -60, −30, 0, +30, +60 mV). The time interval between indentations should be ~3× the time-constant of recovery from inactivation (Fig. 9A, B).
3. Repeat stimulation at the initial holding potential (e.g., +60 mV). If both current amplitudes are not identical (±20%), the stimulation is not reproducible and the measurement should be triaged.
4. Fit current amplitudes as a function of the holding potential with a line to determine the reversal potential. Note that due to intrinsic rectification as well as current run-up/run-down the curve may not be linear throughout and points for the fit should be chosen accordingly. This can be repeated in solutions with different ratios of permeant ions to determine relative permeability using the Nernst equation (Fig. 9C).

*Replication*: Reversal potentials should be based on at least 10 individual cells and 2 individual transfections.

### 3.3.3 Gating kinetics: Activation, deactivation, inactivation, recovery from inactivation

Poke stimulation as a means for measuring gating kinetics of MACs is widely used. However, stimulus adaptation, for example due to relaxation of the indented cell, produces time-dependent changes of membrane tension and indentation forces, leading to highly variable stimulus-responses. Also, the limits of time resolution that poke stimulation achieves are not known a priori, but cannot be faster than the rise time of the indentation step (= actuator speed * step-size; typically ~5–10 ms). Viscoelastic

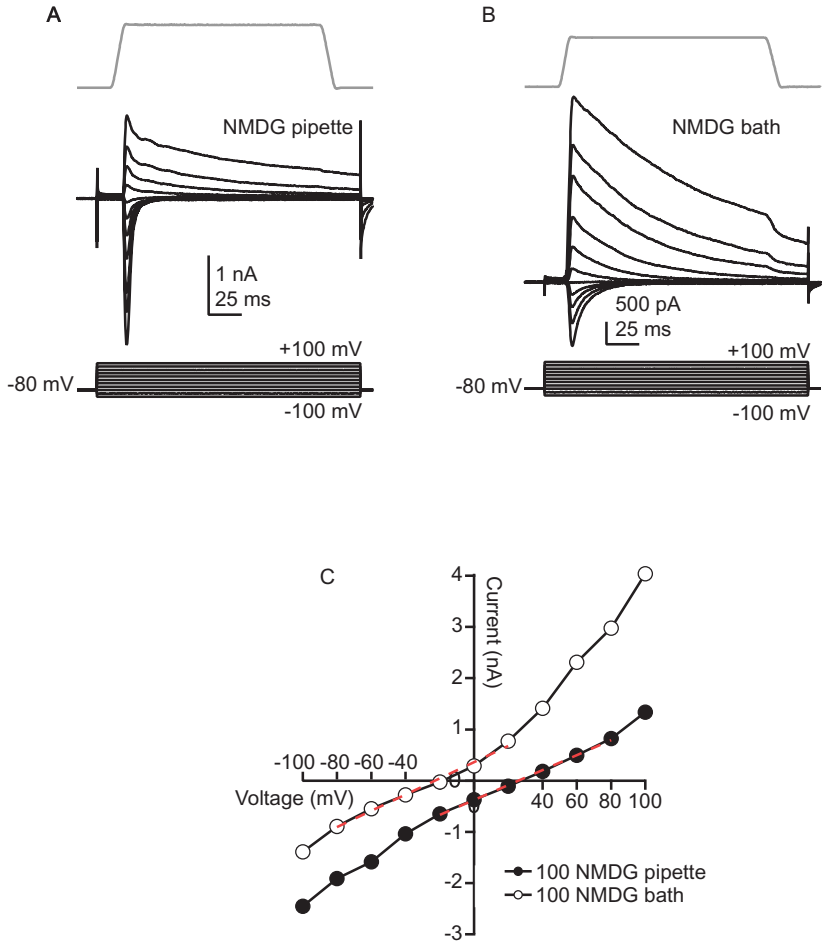


**Fig. 9** Ion selectivity. (A) Indentation stimulus protocol (top), current (middle) and voltage protocol (bottom) from a whole-cell recording from a HEK293t cell expressing mouse Piezo1. 100 mM of the permeant ion in the standard pipette solution was replaced with equimolar NMDG to reduce outward permeation. (B) Stimulus protocol (top), current (middle) and voltage protocol (bottom) from a whole-cell protocol from a HEK293t cell expressing mouse Piezo1. 100 mM of the permeant ion in the standard bath solution was replaced with equimolar NMDG to reduce inward permeation. (C) Current-voltage relationship for the cells in (A) (100 NMDG pipette, closed circles) and (B) (100 NMDG bath, open circles). Because currents can run up and/or down, linear fits (red) were restricted to the five smallest absolute current values, where currents remained linear, and allowed calculation of reversal potentials of +25.9 and −22.7 mV, respectively.

relaxation and the diffusion of membrane tension may further slow the apparent kinetics substantially, but their time constants are not straightforward to assess. Including MACs with fast kinetic time constants as positive controls may enable estimating the limit of time resolution more realistically. For example, for Piezo1 $\tau_a < 1$ ms. In addition, repeated control stimuli can help identify experiments/cells that exhibit excessive adaptation and require triage. Most importantly, the principal limitations of poke stimulation have to be accounted for when interpreting the experimental results (Fig. 10).

**Activation**

1. Apply an indentation step that generates a current amplitude representative of >25 MACs
2. Fit the rising phase of the current with an exponential function to determine the activation time constant ($\tau_a$). If the current inactivates and the time courses of activation and inactivation are similar, the current should instead be fit with a double exponential to avoid contamination of the rising phase by inactivation.
3. Only activation time constants that are much slower (~3×) than the indentation step time truly reflect channel gating (Fig. 10A, B).

**Inactivation**

1. Apply an indentation step that is long compared to the kinetics of overall current decay, ideally resulting in a stable current equilibrium, and that generates a current amplitude representative of >25 MACs.
2. Fit the current decay with one exponential function to determine the time constant of inactivation ($\tau_i$). If the time course of activation is particularly slow, the entire current (rise and decay) may instead need to be fit with a double exponential to properly resolve the two time constants ($\tau_I$ and $\tau_a$) (Fig. 10A–C).

**Deactivation**

1. Apply an indentation step that is sufficient to fully open channels, but short (~1/3×) compared to the time constant of inactivation, if present, and that generates a current amplitude representative of >25 MACs (Fig. 10D–E).
2. Fit the current decay following the indentation step with two exponential functions to determine the time constants of deactivation ($\tau_d$) and inactivation ($\tau_i$). The time constant identical to that determined with the inactivation protocol can be attributed to inactivation and the remaining time constant to deactivation (Fig. 10F). If there is little contribution of inactivation to the decay (for example, at negative potentials for Piezo ion channels), the decay can instead be fit with a single exponential.

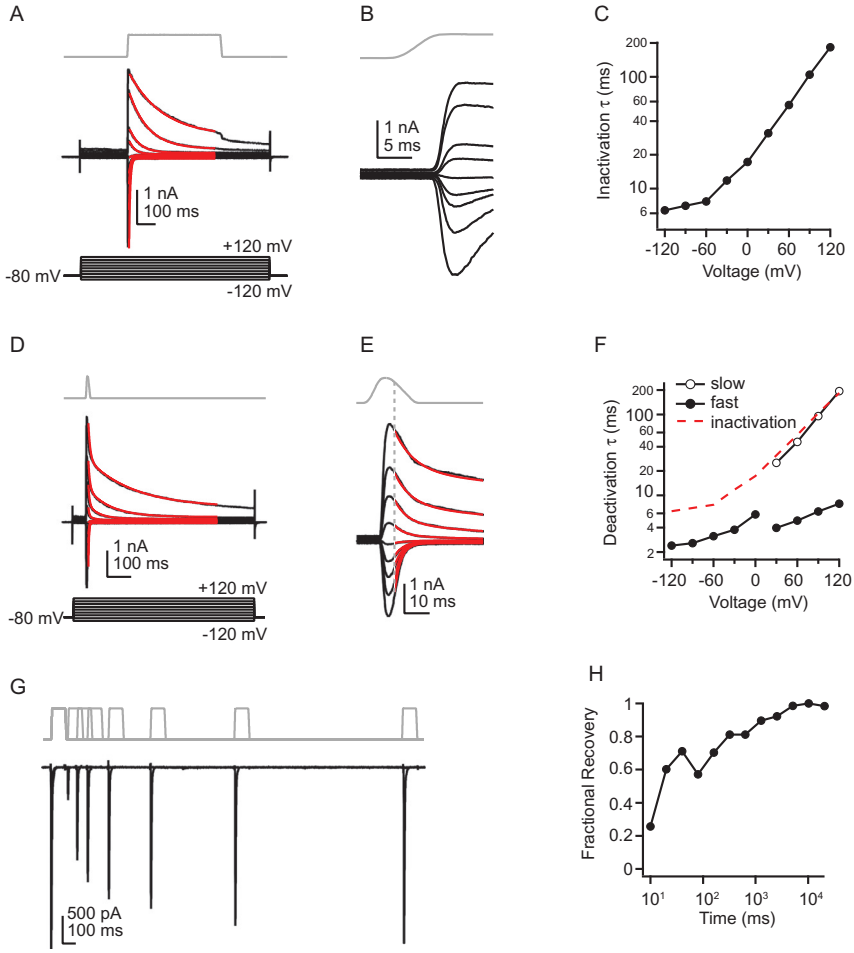


**Fig. 10** Gating kinetics. (A) Indentation stimulus protocol designed to measure inactivation (top), current (middle) and voltage protocol (bottom) from a whole-cell recording from a HEK293t cell expressing mouse Piezo1. Inactivation time constants ($\tau_i$) are obtained by fitting current with a single exponential (red lines). (B) Beginning of the recording from (A) on an expanded time scale. The movement speed of the piezoelectric driver is much slower than that of channel activation, indicating that activation time constants are likely not reflecting channel gating and should be interpreted with caution. (C) Inactivation time constant ($\tau_i$) as a function of voltage for the cell in (A) plotted on a logarithmic scale. (D) Stimulus protocol designed to measure deactivation (top), current (middle) and voltage (bottom) from a whole-cell recording from the same cell as in (A). Deactivation was fit with a single exponential equation for negative voltages and a double exponential equation for positive voltages (red lines). (E) Beginning of the recording from (D) on an expanded time scale. The dashed line indicates the beginning of the fit, during the retraction phase of the piezoelectric driver. (F) Deactivation time constants ($\tau_d$) as a function of voltage for the cell in (D). Note that at positive potentials, the slow component of deactivation overlaps with that of a single exponential fit to inactivation from the same cell (red dashed line). (G) Two-step recovery protocol and whole-cell currents from a HEK293t cell expressing mouse Piezo1. Holding potential was −70 mV. (H) Fractional current recovery, calculated as peak current amplitude upon the second stimulus normalized to peak current amplitude upon the first stimulus, plotted on a logarithmic scale.

3. Ideally, deactivation time constants that are much slower (~3 ×) than the retraction step time truly reflect channel gating. However, channels likely begin deactivating during retraction of the poker, especially if the poker was positioned particularly high above the cell; this point can be visually identified as an inflection point in the current decay and the fit started here.

**Recovery from inactivation**

1. Apply pairs of two stimuli at decreasing time intervals (Fig. 10G). This approach provides an opportunity for detecting run-up or run-down of channel activity unrelated to inactivation and can be used to triage experiments. It is important that the stimulus intervals span a wide range of durations and comprise values that are both much shorter and much longer than the observed time constant of recovery (Fig. 10H). We recommend a minimum of 7 different intervals, spanning at least two orders of magnitude (e.g., 10, 20, 40, 80, 160, 320, 640, 1280 ms).
2. Fit the peak current amplitudes as a function of time intervals with single exponential, or multiple exponentials if the relationship is clearly multi-phasic.

*Replication*: Time constants of gating kinetics should be based on at least 10 individual cells and 2 individual transfections.

## Acknowledgments

This work was supported by NIH R01-NS110552. We thank members of the Grandl lab for thoughtful comments.

## References

Awayda, M. S., Ismailov, I. I., Berdiev, B. K., & Benos, D. J. (1995). A cloned renal epithelial Na+ channel protein displays stretch activation in planar lipid bilayers. *The American Journal of Physiology*, *268*(6 Pt 1), C1450–C1459. https://doi.org/10.1152/ajpcell.1995.268.6.C1450.

Besch, S. R., Suchyna, T., & Sachs, F. (2002). High-speed pressure clamp. *Pflügers Archiv*, *445*(1), 161–166. https://doi.org/10.1007/s00424-002-0903-0.

Coste, B., Crest, M., & Delmas, P. (2007). Pharmacological dissection and distribution of NaN/Nav1.9, T-type Ca2+ currents, and mechanically activated cation currents in different populations of DRG neurons. *The Journal of General Physiology*, *129*(1), 57–77. https://doi.org/10.1085/jgp.200609665.

Coste, B., Murthy, S. E., Mathur, J., Schmidt, M., Mechioukhi, Y., Delmas, P., et al. (2015). Piezo1 ion channel pore properties are dictated by C-terminal region. *Nature Communications*, *6*, 7223. https://doi.org/10.1038/ncomms8223.

Deng, Z., Maksaev, G., Schlegel, A. M., Zhang, J., Rau, M., Fitzpatrick, J. A. J., et al. (2020). Structural mechanism for gating of a eukaryotic mechanosensitive channel of small conductance. *Nature Communications*, *11*(1), 3690. https://doi.org/10.1038/s41467-020-17538-1.

Dubin, A. E., Murthy, S., Lewis, A. H., Brosse, L., Cahalan, S. M., Grandl, J., et al. (2017). Endogenous Piezo1 can confound mechanically activated channel identification and characterization. *Neuron*, *94*(2), 266–270. https://doi.org/10.1016/j.neuron.2017.03.039.

Gamper, N., & Rohacs, T. (2012). Phosphoinositide sensitivity of ion channels, a functional perspective. *Sub-Cellular Biochemistry*, *59*, 289–333. https://doi.org/10.1007/978-94-007-3015-1_10.

Hao, J., & Delmas, P. (2011). Recording of mechanosensitive currents using piezoelectrically driven mechanostimulator. *Nature Protocols*, *6*(7), 979–990. https://doi.org/10.1038/nprot.2011.343.

Jia, Y., Zhao, Y., Kusakizako, T., Wang, Y., Pan, C., Zhang, Y., et al. (2020). TMC1 and TMC2 proteins are pore-forming subunits of mechanosensitive ion channels. *Neuron*, *105*(2), 310. 321 e313. https://doi.org/10.1016/j.neuron.2019.10.017.

Lewis, A. H., & Grandl, J. (2015). Mechanical sensitivity of Piezo1 ion channels can be tuned by cellular membrane tension. *eLife*, *4*. https://doi.org/10.7554/eLife.12088.

Murthy, S. E., Dubin, A. E., Whitwam, T., Jojoa-Cruz, S., Cahalan, S. M., Mousavi, S. A. R., et al. (2018). OSCA/TMEM63 are an evolutionarily conserved family of mechanically activated ion channels. *eLife*, 7. https://doi.org/10.7554/eLife.41844.

Patel, A. J., Honore, E., Maingret, F., Lesage, F., Fink, M., Duprat, F., et al. (1998). A mammalian two pore domain mechano-gated S-like K+ channel. *The EMBO Journal*, *17*(15), 4283–4290. https://doi.org/10.1093/emboj/17.15.4283.

Poole, K., Herget, R., Lapatsina, L., Ngo, H. D., & Lewin, G. R. (2014). Tuning piezo ion channels to detect molecular-scale movements relevant for fine touch. *Nature Communications*, *5*, 3520. https://doi.org/10.1038/ncomms4520.

Prieto, M. L., Firouzi, K., Khuri-Yakub, B. T., & Maduke, M. (2018). Activation of Piezo1 but not NaV1.2 channels by ultrasound at 43 MHz. *Ultrasound in Medicine & Biology*, *44*(6), 1217–1232. https://doi.org/10.1016/j.ultrasmedbio.2017.12.020.

Ranade, S. S., Qiu, Z., Woo, S. H., Hur, S. S., Murthy, S. E., Cahalan, S. M., et al. (2014). Piezo1, a mechanically activated ion channel, is required for vascular development in mice. *Proceedings of the National Academy of Sciences of the United States of America*, *111*(28), 10347–10352. https://doi.org/10.1073/pnas.1409233111.

Slavchov, R. I., Nomura, T., Martinac, B., Sokabe, M., & Sachs, F. (2014). Gigaseal mechanics: Creep of the gigaseal under the action of pressure, adhesion, and voltage. *The Journal of Physical Chemistry. B*, *118*(44), 12660–12672. https://doi.org/10.1021/jp506965v.

Sokabe, M., Sachs, F., & Jing, Z. Q. (1991). Quantitative video microscopy of patch clamped membranes stress, strain, capacitance, and stretch channel activation. *Biophysical Journal*, *59*(3), 722–728. https://doi.org/10.1016/S0006-3495(91)82285-8.

Suchyna, T. M., Markin, V. S., & Sachs, F. (2009). Biophysics and structure of the patch and the gigaseal. *Biophysical Journal*, *97*(3), 738–747. https://doi.org/10.1016/j.bpj.2009.05.018.

Sukharev, S. I., Martinac, B., Arshavsky, V. Y., & Kung, C. (1993). Two types of mechanosensitive channels in the Escherichia coli cell envelope: Solubilization and functional reconstitution. *Biophysical Journal*, *65*(1), 177–183. https://doi.org/10.1016/S0006-3495(93)81044-0.

Taberner, F. J., Prato, V., Schaefer, I., Schrenk-Siemens, K., Heppenstall, P. A., & Lechner, S. G. (2019). Structure-guided examination of the mechanogating mechanism of PIEZO2. *Proceedings of the National Academy of Sciences of the United States of America*, *116*(28), 14260–14269. https://doi.org/10.1073/pnas.1905985116.

Wu, J., Goyal, R., & Grandl, J. (2016). Localized force application reveals mechanically sensitive domains of Piezo1. *Nature Communications*, 7, 12939. https://doi.org/10.1038/ncomms12939.

Ye, J., Tang, S., Meng, L., Li, X., Wen, X., Chen, S., et al. (2018). Ultrasonic control of neural activity through activation of the Mechanosensitive Channel MscL. *Nano Letters*, *18*(7), 4148–4155. https://doi.org/10.1021/acs.nanolett.8b00935.